Electronic Supplementary Material (ESI) for Nanoscale.
This journal is © The Royal Society of Chemistry 2020

Modulation of field-like spin orbit torque in heavy metal / ferromagnet heterostructure

Zilu Wang[a,b,c], Houyi Cheng[a,c], Kewen Shi[a,*], Yang Liu[a], Junfeng Qiao[a], Daoqian Zhu[a], Wenlong Cai[a], Xueying Zhang[a,b], Sylvain Eimer[a,c], Dapeng Zhu[a,b], Jie Zhang[a], Albert Fert[a,d] and Weisheng Zhao[a,b,c,†]

Corresponding Authors: *shikewen@buaa.edu.cn; †weisheng.zhao@buaa.edu.cn

[a] *Fert Beijing Institute, BDBC, School of Microelectronics, Beihang University, Beijing, China.*

[b] *Beihang-Goertek Joint Microelectronics Institute, Qingdao Research Institute, Beihang University, Qingdao, China.*

[c] *Hefei Innovation Research Institute, Beihang University, Hefei 230013, China*

[d] *Unité Mixte de Physique, CNRS, Thales, University of Paris-Saclay, Palaiseau, France.*

Supplementary material

1. Resistivity measurement of sample series I and II

To verify the perpendicular magnetic anisotropy of the samples, we also measure the anomalous Hall resistance (R_{AHE}) of sample series I and II. R_{AHE} is extracted from $R_{AHE} = V_{xy}/I_x$. By comparing Fig. S1 with Fig. 1(e) and 1(f), the magnitude of R_{AHE} and coercivity shows a similar trend with M_S.

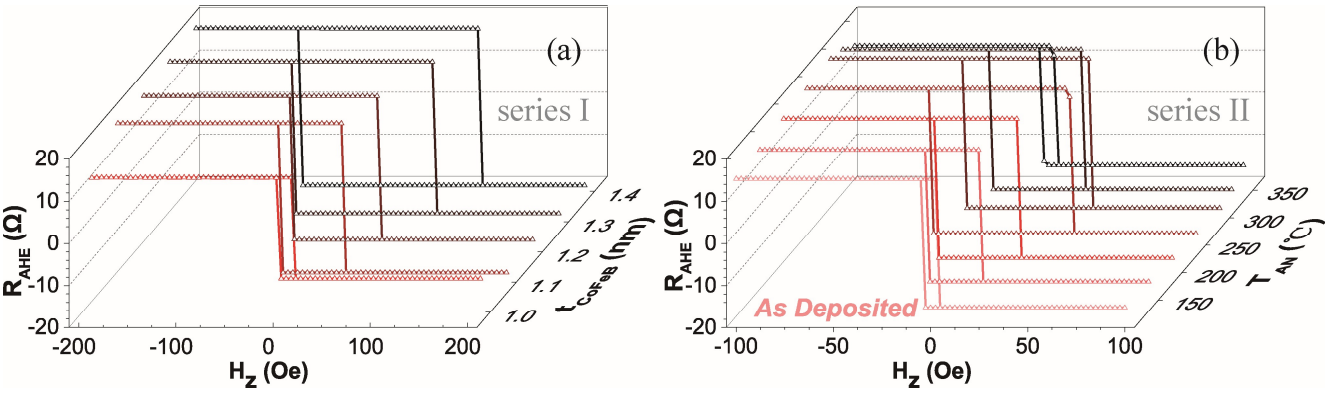

Figure S1. Anomalous Hall resistance (R_{AHE}) of sample series I (a) and II (b). A small non-zero average value of R_{AHE} brought by the small misalignment of the two voltage channels is removed.

We measure the longitudinal conductance (σ_{XX}) of sample series I and II. As illustrated in Fig. S2(a), σ_{XX} is extracted by $\sigma_{XX} = I/V_{XX}$. The resistivities of W and CoFeB are evaluated from the slope and intercept of the linear fitting in sample series I. $\rho_W = 183\ \mu\Omega\ cm$ and $\rho_{CoFeB} = 180\ \mu\Omega\ cm$. As shown in Fig. S2(b), the resistance keeps approximately a constant during annealing.

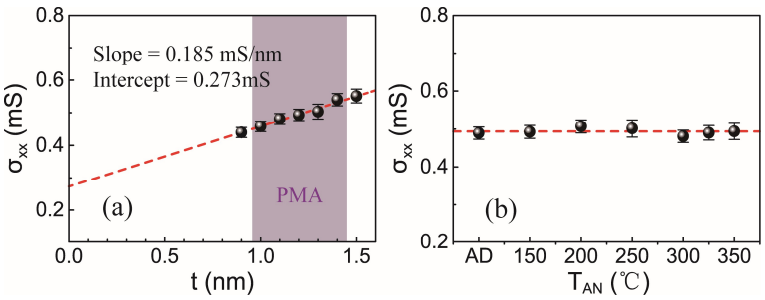

Figure S2. Conductivity of sample series I (a) and II (b). Every data point is an average of 3~7 hall bar structures.

2. Formula derivation of SMR measurement

Considering the longitudinal spin absorption of the FM layer, the SMR ratio $\Delta R_W^{XX}/R_W^{XX}(0)$ can be expressed by following equation (shunting effect term is removed by considering only the HM layer

resistance):[1,2]

$$\frac{\Delta R_W^{XX}(\beta)}{R_W^{XX}(z)} = -\theta_{SH}^2 \frac{\lambda_{HM}}{t_{HM}} \tanh^2(t_{HM}/2\lambda_{HM}) \times \left[\frac{g_R}{1+g_R \coth(t_{HM}/\lambda_{HM})} - \frac{g_F}{1+g_F \coth(t_{HM}/\lambda_{HM})}\right]$$

$$g_R \equiv 2\rho_{HM}\lambda_{HM}G_r,\ g_F \equiv \frac{(1-P^2)\rho_{HM}\lambda_{HM}}{\rho_{FM}\lambda_{FM}\coth(t_{FM}/\lambda_{FM})} \quad \text{(S1)}$$

, where λ_{HM}, t_{HM} and ρ_{HM} are the spin diffusion length, thickness and resistivity of the HM layer. P, λ_{FM}, t_{FM} and ρ_{FM} are the spin polarization, spin diffusion length, thickness and resistivity of the FM layer. $R_W^{XX}(z)$ is the W resistance when m points ±z directions. The first term in bracket is the major source of SMR caused by variation of interfacial spin transfer torque. Its strength is related to both the efficiency of current-spin conversion (θ_{SH}) and spin mixing conductance (G_r). Since θ_{SH} of each sample series keeps a constant, the SMR ratio dominantly reflects effective G_r in our experiment. The second term in bracket represents a slight reduction of SMR caused by longitudinal spin current absorption, whose amplitude increases with t_{FM}.[2] Since $\Delta R_W^{XX}/R_W^{XX}(0)$ increases monotonously with t_{CoFeB} in sample series I, we verify that this slight reduction caused by longitudinal spin current absorption is not the dominant source of SMR variation in our experiment. The effective interfacial spin transparency T_{int}, which is the proportion of spin transfer torque in total spin generation $\theta_{DL}^{ST}/\theta_{SH}$, has a positive correlation with the effective G_r,

$$T_{int} = \mathrm{Re}\left\{\frac{2G_{\uparrow\downarrow}\tanh(t_{HM}/\lambda_{HM})}{\sigma_{HM}/\lambda_{HM}+2G_{\uparrow\downarrow}\coth(t_{HM}/\lambda_{HM})}\right\} \quad \text{(S2)}$$

, where σ_{HM} is the conductivity of the HM layer.

We notice that in Ref. 3, V. L. Grigoryan et al. predicted that the Rashba effect also contributes to a SMR. Since the strength of ISOC and Rashba effect may vary during annealing,[4] our current explanation of SMR data may be disproved. However, we point out that, if the strengthen or weakening of Rashba effect is the dominant source of SMR variation in our annealing experiment, it will lead to the improvement or reduction of the efficiency of current-spin conversion (θ_{SH}). As a result, both the DL and FL torque will increase or decrease simultaneously, which is not the case in our experiment.

3. Anomalous Hall magnetoresistance in single CoFeB layer

Y. Yang et al. reported that there exists a novel kind of magnetoresistance called anomalous Hall magnetoresistance (AHMR) in FM single layer among y-z plane.[5] We tested longitudinal AHMR in single CoFeB layers of 4 nm and 8 nm under 100 μA DC current and 3 T external field rotating inside y-z plane. As

shown in Fig. S3, the AHMR of 8 nm CoFeB is ~ 0.0145 % and AHMR of 4 nm CoFeB is ~ 0.0048 %, which is negligible compared to the SMR observed in W/CoFeB/MgO.

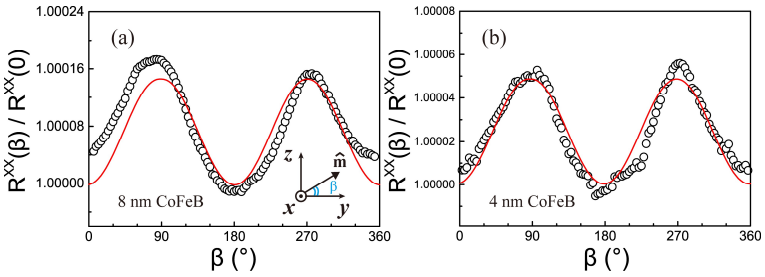

Figure S3. Longitudinal AHMR measured in single CoFeB layer of 8 nm (a) and 4 nm (b). The inset shows the rotation of magnetization. The red lines show the sinusoidal fitting.

4. Details of harmonic measurement

Longitudinal (transverse) SOT effective field ΔH_x (ΔH_y) can be detected by using a standard harmonic measurement.[6,7] We first measure the R_{PHE} under 100 μA DC currect while a 6 T external field rotating inside the *x*-*y* plane. Fig. S4(a) shows the R_{PHE} and sinusoidal fitting measured in W(1.5)/CoFeB(1.1)/MgO(2)/Ta(1.5), T_{AN} = 300 ℃.

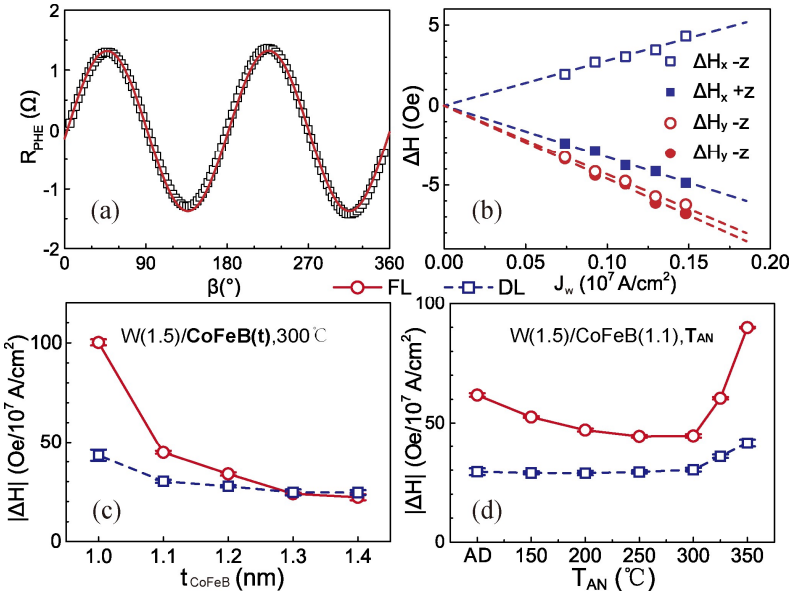

Figure S4. (a) Planar Hall resistance (R_{PHE}) of W(1.5)/CoFeB(1.1)/MgO(2)/Ta(1.5), T_{AN} = 300 ℃. (b) Transverse and longitudinal effective fields as a function of current density of W. (c) and (d) FL and DL effective fields of sample series I and II. Error bars come from the linear fitting of ΔH as a function of current density.

ΔH_x (ΔH_y) is extracted from the parabolic and linear fit of 1st (V_ω) and 2nd ($V_{2\omega}$) harmonic voltage using the following equation considering planar hall effect (PHE) correction:

$$\Delta H_{x(y)} = -\frac{(B_{x(y)} \pm 2rB_{y(x)})}{1-4r^2},\ B_{x(y)} \equiv 2\left(\frac{\partial V_{2\omega}}{\partial H_{x(y)}}\right) / \left(\frac{\partial^2 V_\omega}{\partial H_{x(y)}{}^2}\right) \quad \text{(S3)}$$

, where ± stands for ±z magnetization directions, r is the ratio between PHE resistance (R_{PHE}) and R_{AHE}, H_x (H_y) is an external magnetic field sweeping along x (y) direction. The frequency of the adopted AC current is 133.33Hz. We tilted the sample by 2~4° to give a small out of plane external field in order to prevent multi-domain formation. The average value of the effective fields extracted with the magnetization pointing ±z direction with a small tilt angle can be a good approximation of the actual value.[8] The current density in W layer is calculated by

$$J_W = J \cdot \frac{\rho_{CoFeB}/t_{CoFeB}}{\rho_{CoFeB}/t_{CoFeB} + \rho_W/t_W} \quad \text{(S4)}$$

, where J and J_W are the current density flowing through the full stack and the W layer respectively, and t_W is the W thickness. Fig. S4(b) shows the obtained SOT effective field under different current density. ΔH_x (DL) and ΔH_y (FL) (per 10^7A/cm^2) are extracted from the linear fitting of the effective field. Fig. S4(c) and 4(d) summarize the SOT effective field of sample series I and II. We can find that ΔH_x and ΔH_y are both reduced by larger magnetization. With the same SOT efficiency, SOT effective field is inversely proportional to the magnetization.

References

1 T. J. Peterson, P. Sahu, D. Zhang, M. Dc and J.-P. Wang, *IEEE Trans. Magn.* 2019, **55**, 4100204.

2 J. Kim, P. Sheng, S. Takahashi, S. Mitani and M. Hayashi, *Phys. Rev. Lett.* 2016, **116**, 097201.

3 V. L. Grigoryan, W. Guo, G. E. W. Bauer and J. Xiao, *Phys. Rev. B* 2014, **90**, 161412.

4 L. Zhu, D. C. Ralph and R. A. Buhrman, *Phys. Rev. Lett.* 2019, **122**, 077201.

5 Y. Yang, Z. Luo, H. Wu, Y. Xu, R. W. Li, S. J. Pennycook, S. Zhang and Y. Wu, *Nat. Commun.* 2018, **9**, 2255.

6 J. Kim, J. Sinha, M. Hayashi, M. Yamanouchi, S. Fukami, T. Suzuki, S. Mitani and H. Ohno, *Nat. Mater.* 2013, **12**, 240.

7 K. Garello, I. M. Miron, C. O. Avci, F. Freimuth, Y. Mokrousov, S. Blügel, S. Auffret, O. Boulle, G. Gaudin and P. Gambardella, *Nat. Nanotechnol.* 2013, **8**, 587.

8 P. He, X. P. Qiu, V. L. Zhang, Y. Wu, M. H. Kuok and H. Yang, *Adv. Electron. Mater.* 2016, **2**, 1600210.